On the dynamic nature of azimuthal thermoacoustic modes in annular gas turbine combustion chambers

Nicolas Noiray and Bruno Schuermans

Alstom Power, Baden, Switzerland

Abstract

This paper deals with the dynamics of standing and rotating azimuthal thermoacoustic modes in annular combustion chambers. Simultaneous acoustic measurements have been made at multiple circumferential positions in an annular gas turbine combustion chamber. A detailed statistical analysis of the spatial Fourier amplitudes extracted from these data reveals that the acoustic modes are continously switching between standing, clockwise and counter clockwise traveling waves. A theoretical framework from which the modal dynamics can be explained is proposed and supported by real gas turbine data. The stochastic differential equations that govern these systems have been derived and used as a basis for system identification of the measured engine data. The model describes the probabilities of the two azimuthal wave components as a function of the random source intensity, the asymmetry in the system and the strength of the thermo-acoustic interaction. The solution of the simplified system is in good agreement with experimental observations on a gas turbine combustion chamber.

Keywords: Thermoacoustics; Combustion; Gas turbine; Stochastic Hopf bifurcation; Van der Pol

1. Introduction

In gas turbine combustors, thermoacoustic couplings can yield self-sustained dynamic pressure oscillations which are unwanted because they induce structural vibrations of the combustion chamber's components. This phenomenon is induced by constructive interactions between the flames and the acoustic field which occur when heat release and pressure fluctuations satisfy a phase difference relationship referred to as the Rayleigh's criterion (1896). For annular combustion chambers constituting a widespread design strategy (e.g. Eroglu *et al.* 2009), these acoustic limit cycles often correspond to azimuthal modes. In these situations the combustion chamber circumference is a multiple of the mode wavelength. Several numerical, experimental or theoretical studies have been dedicated to these azimuthal thermoacoustic modes over the last decade in order to better understand and control them to further increase the operational flexibility of the gas turbines.

This is a pre-print version. Published in *Proceedings of the Royal Society A* (2013) Volume 469, Issue 2151, Article number 20120535, DOI: 10.1098/rspa.2012.0535

Based on practical observations, [12] and [34] concluded from *time-averaged* measurements that both dominantly standing or rotating modes can be found depending on the gas turbine operating conditions or burners arrangement. Other studies carried out using low-order thermoacoustic network simulations (see Evesque *et al.* 2003; Schuermans *et al.* 2006; Morgans and Stow 2007; Stow and Dowling 2009) or deriving nonlinear analytical models (Schuermans *et al.* 2006; Noiray *et al.* 2011) shed some light on the dynamic nature of the azimuthal modes. In particular, it is predicted that for a uniform distribution of identical flames along the circumference of the chamber, the thermoacoustic coupling yields rotating type limit cycles due to modal coupling induced by flame response nonlinearities.

The main steps of the analytical approach proposed by [24] are now shortly recalled. Considering the periodic nature of annular geometries, it is natural to decompose the acoustic pressure field p as a Fourier series:

$$p(r,\theta,z,t) = \sum_{m=1}^{\infty} \mu_{m,a}(t)\, f_m(r,z)\, \cos(m\theta) + \mu_{m,b}(t)\, f_m(r,z)\, \sin(m\theta), \tag{1}$$

$$p(\theta,t) = \sum_{m=1}^{\infty} \eta_{m,a}(t)\, \cos(m\theta) + \eta_{m,b}(t)\, \sin(m\theta), \tag{2}$$

where t, θ, r and z are the time, the azimuthal angle, the radial and axial coordinate. The function $f_m(r,z)$ describes the dependence of the acoustic field in radial and axial direction. The time-dependent Fourier coefficients are denoted by $\mu_{m,a}$ and $\mu_{m,b}$. The focus of this study is the azimuthal dependence of the acoustic field. Because all measurements and analysis in this paper are done for one fixed value of r and z, the definitions $\eta_{m,a}(t) = \mu_{m,a}(t)\, f_m(r,z)$ and $\eta_{m,b}(t) = \mu_{m,b}(t)\, f_m(r,z)$ will be used in the remainder of this paper.

The temporal Fourier transforms of $\eta_{m,a}(t)$ and $\eta_{m,b}(t)$ generally show multiple distinct maxima. The frequencies at which these maxima occur are associated with the acoustic modes of the annular combustion chamber.

The flames which are distributed along the circumference can interact constructively with the combustion chamber's acoustics. In this case the system can be brought onto a limit cycle. This is usually characterized by one pair of dominant azimuthal Fourier coefficients $\eta_{n,a}(t)$ and $\eta_{n,b}(t)$, with a dominant limit cycle frequency ω_n. This type of behaviour is typical of weakly damped/amplified oscillators which feature two different time scales: the oscillation frequency $T_n = 2\pi/\omega_n$ and the relaxation time which is associated to the dynamics of the amplitude variations and which is much longer than T_n. Therefore the space–time dependence of the acoustic field can be reasonably approximated by:

$$p(\theta,t) \simeq \eta_a(t)\, \cos(n\theta) \,+\, \eta_b(t)\, \sin(n\theta). \tag{3}$$

with

$$\eta_a(t) = A(t)\cos(\omega_n t + \varphi_a(t)) \tag{4}$$

$$\eta_b(t) = B(t)\cos(\omega_n t + \varphi_b(t)) \tag{5}$$

This is a pre-print version. Published in *Proceedings of the Royal Society A* (2013) Volume 469, Issue 2151, Article number 20120535, DOI: 10.1098/rspa.2012.0535

where A, B, φ_a and φ_b are slowly varying functions with respect to the angular frequency ω_n. It is convenient to make use of the phase difference $\phi = \varphi_a - \varphi_b$ in order to best characterize the modal dynamics. Note that the envelopes A and B can be extracted by taking the Hilbert transform of η_a and η_b as it will be done in the following sections.

Using a deterministic approach, [24] shown that when the flames are identical and uniformly distributed along the annular combustion chamber, the stable limit cycle is given by $A(t) = B(t) = A_0$ and $\phi(t) = \pm\pi/2 \pmod{2\pi}$ which corresponds to a purely left or right spinning mode:

$$p(\theta, t) = A_0 \cos(\omega_n t \pm n\theta). \tag{6}$$

It is also shown in that study that mixed-type standing/spinning ($A \neq B$) modes or even purely standing modes ($A = 0$) or ($B = 0$) will establish in the annular combustion chamber if the coupling strength is not uniform along the circumference. Note that these predictions are in agreement with the ones from [19] which are obtained by considering eigenvalue degeneracy due to the action of a symmetry group (see also Moeck *et al.* 2010 and Moeck 2010).

Recently, these conclusions are open again to question by [28] (see also [42]) as a result of Large Eddy Simulations of a full annular combustion chamber. One can besides refer to [37] and [41]. In the work from [28] and [42], the simulated time corresponds to approximately hundred acoustic cycles during which the first azimuthal mode is standing for the first and last forty periods and rotates in between. The authors of the latter studies state that "the underlying mechanisms driving the transition between rotating and standing modes are still not clear". Considering that the simulated operating conditions are kept constant and that the burners are identical and evenly distributed in the annular chamber, the analytical model proposed by [24] has two solutions: purely left and purely right rotating modes. This is in agreement with the studies carried out by [33], [21] and [38] but not consistent with the aforementioned LES results. Nevertheless, it was already mentioned by [24] that this *deterministic* model cannot describe the switching between the different solutions and that the background noise from the turbulent reactive flow might influence significantly the modal dynamics. In this context, the present study aim at reconciling real gas turbine data and theoretical predictions by including into the model the stochastic forcing terms corresponding to the combustion noise.

2. Observations

It is first interesting to present measurements from a real combustor in order to give a better picture of the actual dynamics of the azimuthal modes in annular combustion chambers. This is done for two off-design operating conditions respectively featuring self-sustained acoustic oscillations of the first and second azimuthal acoustic modes. Indeed for each of these cases, there is one mode which dominates the acoustic spectrum as exemplified in figure 1 for the operating condition where the first azimuthal acoustic mode governs the acoustic signature of the chamber. Dynamic pressure sensors were implemented in the combustion chamber at different azimuthal positions but identical

This is a pre-print version. Published in *Proceedings of the Royal Society A* (2013) Volume 469, Issue 2151, Article number 20120535, DOI: 10.1098/rspa.2012.0535

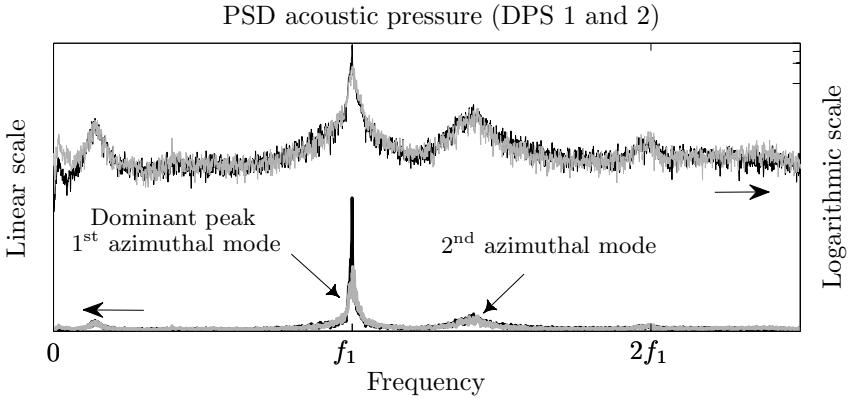

Figure 1: Power spectral densities of the acoustic signals recorded with the dynamic pressure sensors DPS 1 and 2 (black and grey respectively) at the off-design operating condition for which the 1st azimuthal acoustic mode governs the acoustic field.

axial and radial positions as shown in fig. 2(a) and 2(d). Taking the signals from these sensors it is possible to extract the time resolved Fourier components η_a and η_b corresponding to the dominant mode by using the following approximation:

$$\eta_a(t) = \frac{1}{\pi}\int_{-\pi}^{+\pi} p(\theta,t)\cos(n\theta)\,d\theta \;\approx\; \frac{2}{K}\sum_{k=1}^{K} p(\theta_k,t)\cos(n\theta_k) \tag{7}$$

$$\eta_b(t) = \frac{1}{\pi}\int_{-\pi}^{+\pi} p(\theta,t)\sin(n\theta)\,d\theta \;\approx\; \frac{2}{K}\sum_{k=1}^{K} p(\theta_k,t)\sin(n\theta_k) \tag{8}$$

Note that the azimuthal origin is chosen such that the coherence between the Fourier components is minimized in order to properly identify the principal axes of the modes. For the two conditions where the first and second modes respectively govern the system dynamics, the reconstructed pressure fields at arbitrary points in time are shown in fig. 2(a) and 2(d). The raw signals from two of the dynamic pressure sensors are shown in fig. 2(b) and 2(e). The time-resolved slowly varying amplitudes can then be extracted by taking the absolute value of the analytical Fourier coefficients obtained by Hilbert transform: $A(t) = |\eta_a(t) + i\tilde{\eta}_a(t)|$ and $B(t) = |\eta_b(t) + i\tilde{\eta}_b(t)|$. The modal phase difference $\phi(t) = \varphi_a(t) - \varphi_b(t)$ is obtained from $\varphi_a(t) = \arg(\eta_a(t) + i\tilde{\eta}_a(t))$ and $\varphi_b(t) = \arg(\eta_b(t) + i\tilde{\eta}_b(t))$. The slowly varying amplitudes are plotted in fig. 2(b) and 2(e) together with the raw signals over 15 cycles and during a longer interval in fig. 2(c) and 2(f).

A purely standing limit cycle oscillation would be characterised by a constant value of the modal amplitude A and zero amplitude B (or vice versa). A purely rotating mode would be characterised by equal amplitudes A and B with a constant phase difference of $+\pi/2$ for clockwise modes and $-\pi/2$ for counter–clockwise rotating modes. So, it's clear from fig. 2(c) and 2(f) that the acoustic mode is neither a purely standing wave nor a purely rotating mode, but that it features a stochastic switching between modes. This conclusion was already drawn by [24] based on advanced thermoacoustic network simulations of a gas turbine combustor: the intense background noise produced by

This is a pre-print version. Published in *Proceedings of the Royal Society A* (2013) Volume 469, Issue 2151, Article number 20120535, DOI: 10.1098/rspa.2012.0535

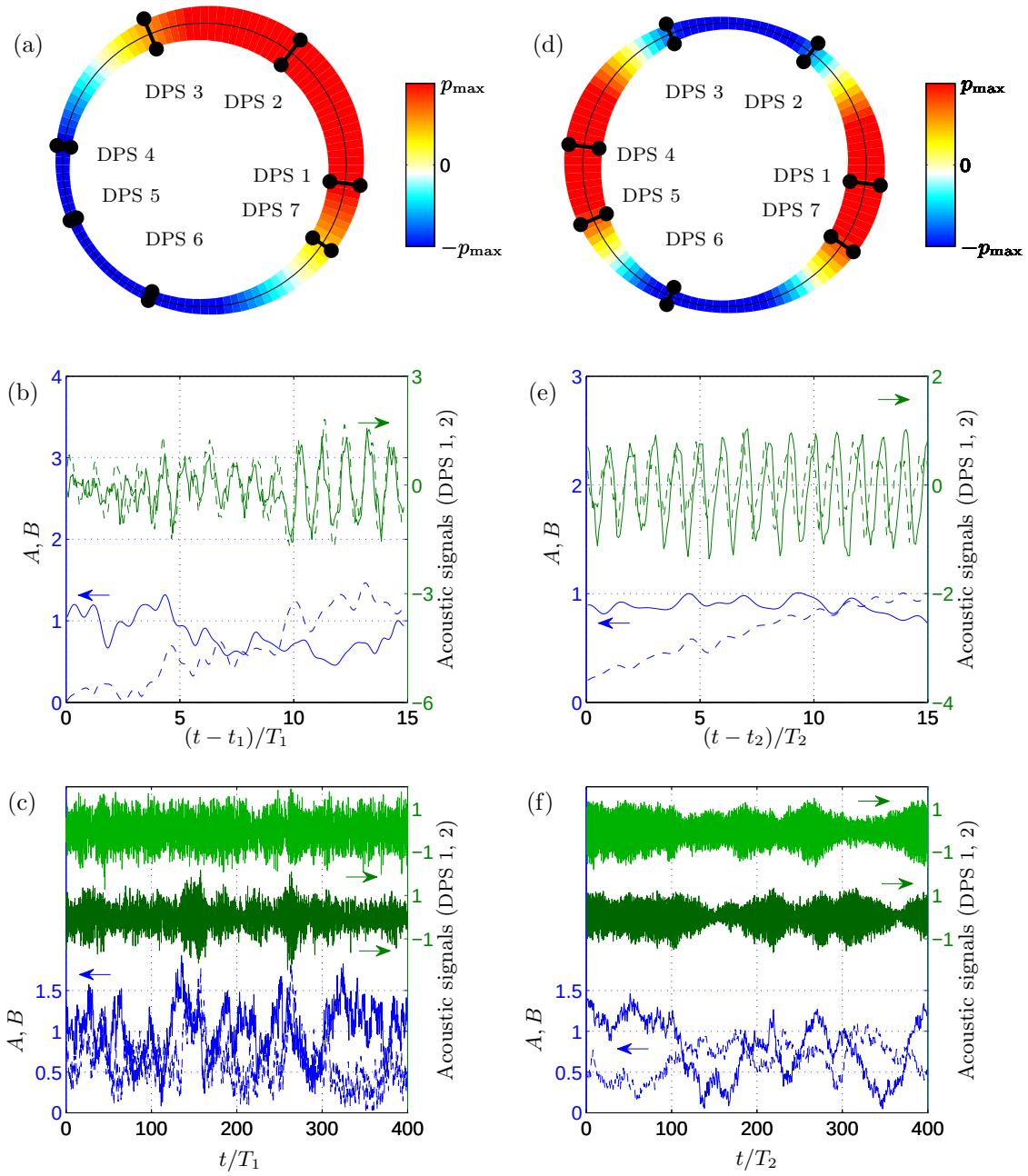

Figure 2: Characteristics of the first and second azimuthal Fourier amplitudes observed in the annular combustion chamber at two different off-design operating conditions (resp. (a) to (c) and (d) to (f)). **Diagrams (a) and (d):** Reconstructed acoustic pressure distribution at a given instant. The black lines are scaled relative to the amplitude of the raw signals measured by means of the seven dynamic pressure sensors (DPS). **Diagrams (b) and (e):** Short samples of the raw signals from DSP 1 and 2 plotted together with the extracted modal amplitudes A and B. **Diagrams (c) and (f):** Same as (b) and (e) on a longer time interval. Time is scaled relative to the acoustic periods $T_1 = 1/f_1$ (see figure 1) and $T_2 = 1/f_2$.

This is a pre-print version. Published in *Proceedings of the Royal Society A* (2013) Volume 469, Issue 2151, Article number 20120535, DOI: 10.1098/rspa.2012.0535

the highly turbulent reactive flow in the combustion chamber dramatically influences the modal dynamics.

In order to get insights into the stochastic behavior of the amplitudes A and B presented in fig. 2(c) and 2(f) and of the phase difference ϕ , the corresponding joint probability distributions are shown in fig. 3. One can see in fig. 3(a) and in fig. 3(c) that for the two off-design operating conditions each characterized by the presence of a dominant self-sustained acoustic mode, the modal amplitudes A and B take values which are spread around a well-defined probability maximum. If this maximum would be located on the diagonal $A = B$ in these figures, then this would indicate that the most probable mode is a rotating mode. A predominantly standing mode would be characterized by a maximum on one of the axes. In these particular configurations, the maximum is neither located on the principal diagonal nor on one of the axis. In the deterministic framework, the case $A \neq B$ can be desribed as a partly standing, partly rotating mode. As it has been shown by [24], this is due to a non-uniform distribution of the acoustic-flame interaction strength.

Note that the spread is wider for the operating condition governed by the first azimuthal mode which can be explained by a relatively stronger background noise. In fig. 3(b) and in fig. 3(d), one can observe that the most probable phase difference ϕ is approximately equal to $\pm\pi/2$. For a hypothetical case where the modal amplitudes would be equal and constant, having a phase difference of plus or minus $\pi/2$ respectively means that the mode spins in the clockwise or counter-clockwise direction. In the case of the dominant second azimuthal mode, one can see that the preferred spinning direction is clearly counter-clockwise. Even though the azimuthal velocity component $\bar{u}_\theta$ is much lower than the axial one $\bar{u}_z$ with $\bar{u}_\theta \ll \bar{u}_z \ll c$, c being the speed of sound, a possible explanation could be the swirl direction of the hot gas flow in the annular chamber.

These observations highlight the unquestionable gap between the fixed amplitudes predicted from the deterministic model and the strongly fluctuating ones observed in a real gas turbine combustion chamber. In the following section, one derives a theoretical model which allows to account for the influence of the background noise and to explain the observations.

3. Theoretical model

The aim of this study is to analyze the modal dynamics in annular combustion chambers subject to thermoacoustic coupling. Therefore a model will be derived that is as simple as possible, but which captures the essential modal dynamics. Note that it is not the aim here to present a model to predict linear stability or limit cycles, but rather to derive a set of equations that describe the observed modal dynamics. Unknown coefficients in the model will then be obtained by means of system identification methods with measured engine data as an input.

In annular combustion chambers, the three dimensional acoustic modes satisfying the Laplace equation which may be used to expand the pressure field can be expressed in polar coordinate as $\psi_{m,a} = f_m(r, z)\cos(m\theta)$ and $\psi_{m,b} = f_m(r, z)\sin(m\theta)$. In order to simplify the equations in the

This is a pre-print version. Published in *Proceedings of the Royal Society A* (2013) Volume 469, Issue 2151, Article number 20120535, DOI: 10.1098/rspa.2012.0535

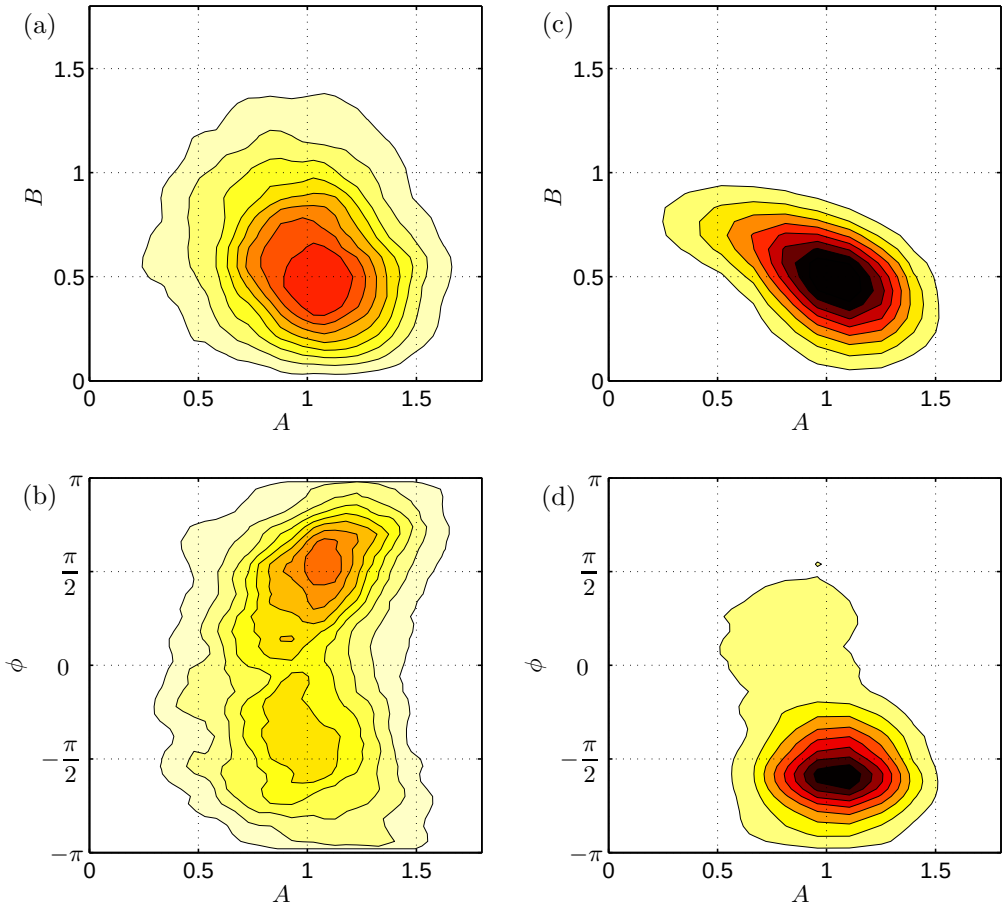

Figure 3: Left and right diagrams correspond to the first and second azimuthal modes observed in the annular combustion chamber at two distinct off-design operating conditions. **Diagrams (a) and (c):** Bivariate density functions of the modal amplitudes A and B (same color scale for (a) and (c)). **Diagrams (b) and (d):** Bivariate density functions of the modal amplitude A and the phase difference ϕ (same color scale for (b) and (d)). The p.d.f. are calculated from signals corresponding to approximately 6000 acoustic periods.

This is a pre-print version. Published in *Proceedings of the Royal Society A* (2013) Volume 469, Issue 2151, Article number 20120535, DOI: 10.1098/rspa.2012.0535

subsequent analysis, for which the focus is put on the azimuthal dynamics of the acoustic field, the radial and axial dependances of $\psi_{m,a}$ and $\psi_{m,b}$ are not considered, i.e. $f_m(r,z)=1$. Nevertheless this analysis can be equally applied to three dimensional modal structures as it is shown by [23]. The following wave equation, including source and damping terms is therefore considered

$$\frac{\partial^2 p}{\partial t^2}+\alpha\frac{\partial p}{\partial t}-\frac{c^2}{R^2}\frac{\partial^2 p}{\partial \theta^2}=\frac{\partial Q}{\partial t}, \tag{9}$$

where α is the damping factor, c the sound speed, R the mean radius of the annular combustor and Q the normalized heat release rate. In practical systems, there can be *locally* considerable temperature gradients, but *globally* the dispersion is negligible for the first azimuthal modes. For instance, in the work from [42] the acoustic pressure is quasi-sinusoidal along the azimuthal coordinate and the influence of the periodic temperature variations between adjacent burners on the wave propagation is not detectable (see figures 5, 7 and 9 in the aforementioned study). One can also refer to [24] for more explanations about this approximation.

Thermoacoustic interaction becomes constructive when a phase relationship between acoustic pressure and fluctuating heat release rate – referred to as Rayleigh criterion – is satisfied. This coupling results from very complex mechanisms linking acoustic waves to flame dynamics via for instance acoustically triggered equivalence ratio fluctuations or vortex-flame interactions. It is often convenient to describe the acoustic-flame coupling in the frequency domain and write that the fluctuating heat release rate depends on the acoustic quantities via a flame transfer function:

$$\hat{Q}=F_u(\omega)\hat{u}+F_p(\omega)\hat{p}, \tag{10}$$

where u is the acoustic velocity. Replacing $\hat{u}$ by $\hat{p}/Z_b$ where Z_b is the burner impedance, one get

$$\hat{Q}=\left(\frac{F_u(\omega)}{Z_b(\omega)}+F_p(\omega)\right)\hat{p}=G(\omega)\hat{p}. \tag{11}$$

The flame transfer function is usually a smooth function. Indeed it is possible to approximate $G(\omega)$ by a complex constant $\beta+i\,\gamma$ for frequencies which are close to some frequency ω_n of interest. This approximation is generally valid on a frequency range extending over the peak width. In the time domain, eq. (11) can therefore be approximated by

$$Q=\beta p+\frac{\gamma}{\omega_n}\frac{\partial p}{\partial t} \tag{12}$$

The first R.H.S. term will act on the damping in (9) and it can be positive or negative respectively making the system linearly unstable or stable. The second term will have an influence on the system's oscillation frequency. This effect will be neglected in the subsequent analysis because in practical systems, the eigenfrequencies of the combustor exhibiting thermoacoustic coupling are very close to the ones of the combustor without heat release source term. One can consequently keep $Q=\beta p$ as a good description of the flame response to acoustic perturbations where β stands for the effective linear dependance and contains the influence of convective delays and

This is a pre-print version. Published in *Proceedings of the Royal Society A* (2013) Volume 469, Issue 2151, Article number 20120535, DOI: 10.1098/rspa.2012.0535

amplification factors of the underlying complex mechanisms. This relationship is valid for the case of small perturbations, however it is known that when the acoustic amplitude become large the heat release rate fluctuations do not follow the excitation and saturation mechanisms take place. For instance, the shear layer receptivity can play a crucial role as demonstrated in the outstanding work reported by [25]. As a first approximation, this nonlinearity can be accounted for using a third order term in the last-mentioned relationship:

$$Q = \beta\, p - \kappa\, p^3. \tag{13}$$

Note that the second and fourth order terms would anyway vanish in the subsequent analysis as shown by [23]. Replacing the expressions for p and Q given in eqs. (3) and (13) into eq. (9), multiplying both sides by $\cos(n\theta)$ and integrating with respect to θ between 0 and 2π, one obtains the autonomous ordinary differential equation governing η_a. Applying the same procedure with $\sin(n\theta)$ yields the one for η_b. The resulting system of coupled nonlinear equations is

$$\ddot{\eta}_a + \omega_n^2\, \eta_a = (\beta - \alpha)\, \dot{\eta}_a - 3\kappa\big(\dot{\eta}_a(3\eta_a^2 + \eta_b^2) + 2\dot{\eta}_b\eta_a\eta_b\big)/4, \tag{14}$$

$$\ddot{\eta}_b + \omega_n^2\, \eta_b = (\beta - \alpha)\, \dot{\eta}_b - 3\kappa\big(\dot{\eta}_b(3\eta_b^2 + \eta_a^2) + 2\dot{\eta}_a\eta_a\eta_b\big)/4, \tag{15}$$

where $\omega_n = nc/R$. The stability of this system as been investigated by [24]. However the conclusions related to the dynamic nature of the eigenmodes are only valid for the case of infinitely small perturbations of the limit cycles. As shown in the previous section, the deterministic approach cannot properly describe the actual modal dynamics encountered in gas turbine combustors. This is why the stochastic forcing produced by the highly turbulent reactive flow must be introduced in the model. Note that the influence of this random excitation on thermo-acoustic couplings has only been considered in a limited number of studies ([6, 15, 40, 23]).

The noise generated by premixed turbulent flames has received attention from many researchers (e.g. the early work from [10]). Most of the reported studies are based on the pioneering contribution from [16] and one can refer to the recent work from [29] to get an in-depth overview on the subject. The noise radiated by turbulent premixed flames is characterized by a power spectrum having a smooth maximum with power law dependences on both sides. In this respect the peaks corresponding to thermo-acoustically driven limit cycles are very narrow and as a first approximation, the stochastic forcing produced by the flames is assumed to act as an additive white noise excitation. One can therefore model realistic nonlinear modal interactions by adding a stochastic forcing into eqs. (14) and (15):

$$\ddot{\eta}_a + \omega_n^2\, \eta_a = \mathcal{G}_a(\dot{\eta}_a, \eta_a, \dot{\eta}_b, \eta_b) + \xi_a, \tag{16}$$

$$\ddot{\eta}_b + \omega_n^2\, \eta_b = \mathcal{G}_b(\dot{\eta}_a, \eta_a, \dot{\eta}_b, \eta_b) + \xi_b. \tag{17}$$

where ξ_a and ξ_b are two uncorrelated white noises of intensity Γ. The fact that these noise sources are additive is demonstrated by [23]. The right hand sides are small compared to the left hand sides – weakly damped/amplified oscillators – and respectively following [13] and [39], one can

This is a pre-print version. Published in *Proceedings of the Royal Society A* (2013) Volume 469, Issue 2151, Article number 20120535, DOI: 10.1098/rspa.2012.0535

apply deterministic and stochastic averaging to eqs. (16) and (17) in order to get the equations for the slowly varying amplitudes and phase:

$$\begin{aligned}
\dot{A} &= \nu A - \frac{3\kappa}{32}\left(3A^2 + (2+\cos 2\phi)B^2\right)A + \frac{\Gamma}{4\omega_n^2 A} + \zeta_a \\
\dot{B} &= \nu B - \frac{3\kappa}{32}\left(3B^2 + (2+\cos 2\phi)A^2\right)B + \frac{\Gamma}{4\omega_n^2 B} + \zeta_b \\
\dot{\phi} &= \frac{3\kappa}{32}\left(A^2+B^2\right)\sin(2\phi) + \left(\frac{1}{A}+\frac{1}{B}\right)\zeta_\phi
\end{aligned} \tag{18}$$

where $\nu = (\beta - \alpha)/2$ is the linear growth rate and ζ_a, ζ_b and ζ_ϕ are uncorrelated white noises of intensity $\Gamma/2\omega_n^2$. One can also refer to the work from [36] and [32] for stochastic averaging in the context of noise driven oscillators. Note that the equation for ϕ results from the difference of the equations for φ_a and φ_b.

4. System identification

The next step consists in checking that the theoretical model fits to the observations. For that purpose, the time limits of the first transition moments of the amplitudes process are calculated from the experimental data. They are then used to perform a parametric system identification based on the stochastic dynamic model proposed in the previous section. This strategy has been for the first time proposed by [35] and recently improved to account for finite sampling rates effects (see Lade 2009 and Honisch and Friedrich 2011). From the work of [11], it is known that these limits are the drift coefficients of the Fokker-Planck equation associated to the coupled system of Langevin equations (18). It is also known that the drift coefficients – or first Kramers-Moyal coefficients – provide the deterministic contribution in the stochastic differential system. In order to ease the subsequent analysis, the change of variables $\{A, B, \varphi_a, \varphi_b\} \rightarrow \{A, B, \check{A}, \check{B}\}$ is made with $\check{A} = (2+\cos 2\phi)^{1/2}A$ and $\check{B} = (2+\cos 2\phi)^{1/2}B$. The first two equations from the system (18) become:

$$\dot{A} = \overbrace{\nu_a A - \frac{3\kappa_a}{32}(3A^2 + \check{B}^2)A + \frac{\Gamma_a}{4\omega_n^2 A}}^{\mathcal{F}_A(A,\check{B})} + \zeta_a \tag{19}$$

$$\dot{B} = \underbrace{\nu_b B - \frac{3\kappa_b}{32}(3B^2 + \check{A}^2)B + \frac{\Gamma_b}{4\omega_n^2 B}}_{\mathcal{F}_B(\check{A},B)} + \zeta_b \tag{20}$$

Note that in the parameter identification process, the linear growth rates, nonlinear coefficients and noise intensity in the amplitude equations can differ from each other in contrast with (18). This is because as shown by [24] for the deterministic case, if there are some azimuthal non uniformities in the thermoacoustic coupling strength, the degenerate eigenvalue will split and the assumption

This is a pre-print version. Published in *Proceedings of the Royal Society A* (2013) Volume 469, Issue 2151, Article number 20120535, DOI: 10.1098/rspa.2012.0535

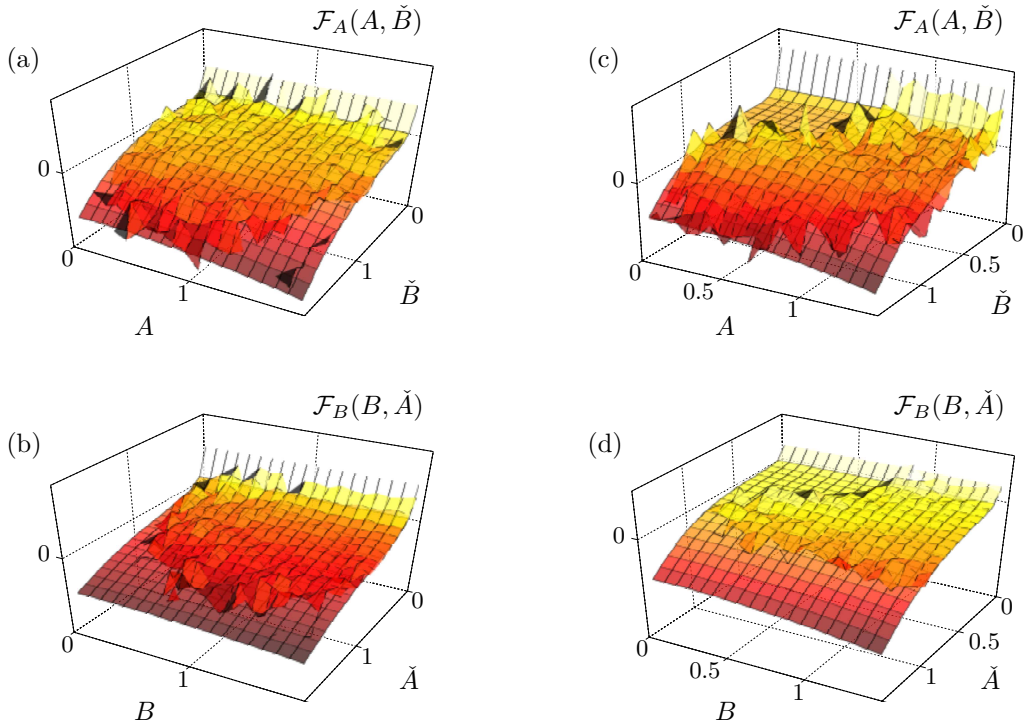

Figure 4: Left and right diagrams respectively correspond to the first and second azimuthal eigenmodes. Drift coefficients corresponding to the deterministic components of the stochastic differential equations governing the modal dynamics. The theoretical best fits are superimposed to the first transition moments time limits calculated from measured data.

$\nu_a = \nu_b = \nu$ will not hold. It is also assumed that the nonlinear coefficients κ_a and κ_b and noise intensity Γ_a and Γ_b might slightly differ from each others. The first Kramers-Moyal coefficients are defined by

$$\lim_{\tau\to 0}\frac{1}{\tau}\iint_{-\infty}^{+\infty}(a-A)\,P\big(\{a,\check{b}\}_{t+\tau}|\{A,\check{B}\}_t\big)\,da\,d\check{b} \;=\; \mathcal{F}_A(A,\check{B}), \tag{21}$$

$$\lim_{\tau\to 0}\frac{1}{\tau}\iint_{-\infty}^{+\infty}(b-B)\,P\big(\{\check{a},b\}_{t+\tau}|\{\check{A},B\}_t\big)\,d\check{a}\,db \;=\; \mathcal{F}_B(\check{A},B), \tag{22}$$

where the conditional probability density $P\big(\{a,\check{b}\}_{t+\tau}|\{A,\check{B}\}_t\big)$ describes the probability that the amplitudes takes values a and $\check{b}$ at time $t+\tau$ under the condition that they have been at A and $\check{B}$ at time t. The coefficients were calculated from the experimental data presented in fig. 2(c) and 2(f) corresponding to the two off-design operating conditions for which the thermoacoustic coupling respectively operates on the first and second azimuthal modes. Note that only a fraction of the data set is presented in these diagrams. The calculated drift coefficients are presented in

This is a pre-print version. Published in *Proceedings of the Royal Society A* (2013) Volume 469, Issue 2151, Article number 20120535, DOI: 10.1098/rspa.2012.0535

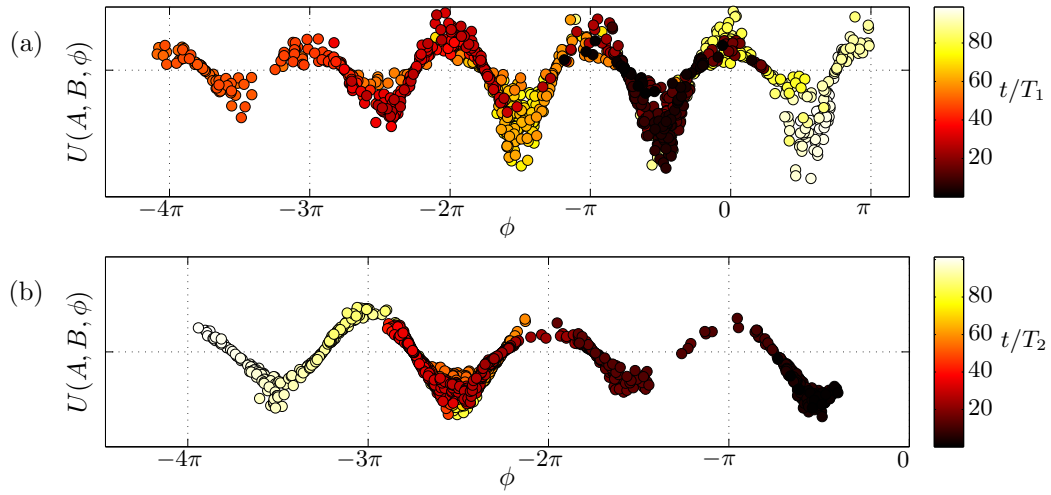

Figure 5: Diagrams (a) and (b) respectively correspond to the first and second azimuthal eigenmodes. Potential U computed from the extracted values of the modal amplitudes A and B and phase difference ϕ during short intervals (100 periods).

fig. 4 together with the best fit from the theoretical model given in eqs. (19) and (20). The fact that one can find parameters ν_a, ν_b, κ_a, κ_b, Γ_a and Γ_b for which the theoretical model matches so well with the measured data is not a proof but a clear indication that the model captures the main features of the actual modal dynamics.

5. Simplified model

To get a better picture of the complex interactions between modal amplitudes and phases, one can concentrate on the phase difference dynamics defined by the third equation of the stochastic differential system (18). This Adler equation with stochastic forcing describes the mutual synchronization of the two eigenmodes $\cos(n\theta)$ and $\sin(n\theta)$. It can be written in the form

$$\dot{\phi} = -\frac{\partial U}{\partial \phi} + \left(\frac{1}{A} + \frac{1}{B}\right)\zeta_\phi, \tag{23}$$

$$\text{with} \quad U(A,B,\phi) = \frac{3\kappa}{64}\left(A^2 + B^2\right)\cos(2\phi), \tag{24}$$

where U is the potential governing the phase difference dynamics. Readers interested by synchronization phenomena can refer to the outstanding contribution from [1]. For given values of A and B, the corresponding minima are at $\phi = \pm\pi/2 \pmod{2\pi}$. Based on the extracted values of A, B and ϕ presented in fig. 2(c) and 2(f), the time resolved potential U has been calculated for a short interval. Results are presented in fig. 5. One can see that ϕ takes all values over the range $[-\pi, \pi] \pmod{2\pi}$ but it stays longer in the potential wells. Indeed, the phase difference locks for some

This is a pre-print version. Published in *Proceedings of the Royal Society A* (2013) Volume 469, Issue 2151, Article number 20120535, DOI: 10.1098/rspa.2012.0535

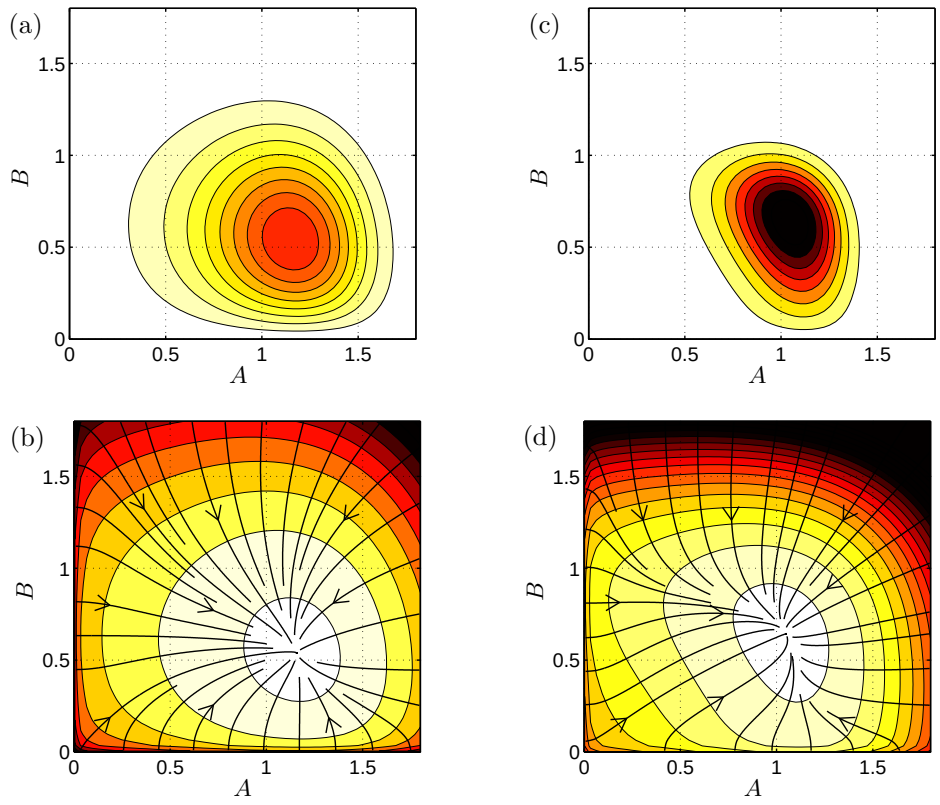

Figure 6: Left and right diagrams respectively correspond to the first and second azimuthal eigenmodes. **Diagrams (a) and (c):** Bivariate density functions of the modal amplitudes A and B calculated from the simplified potential version of the coupled system given by eq. (27). The color scale for (a) and (c) is the same as the one used in subfigures 2(a) and 2(c). **Diagrams (b) and (d):** Corresponding potentials given by eq. (26).

time on a value close to $\pm\pi/2 \pmod{2\pi}$ before being kicked out and falling in another well due to the amplitude dependent stochastic forcing. This synchronization phenomenon is explained by the fact that in spite of the intense forcing, the system tends to stay close to the stable deterministic limit cycle solutions.

It is also interesting to focus on the dynamics of the modal amplitudes A and B. Given that the phase difference often takes values close to $\pm\pi/2 \pmod{2\pi}$ and that the best fit parameters from the previous section are such that $\kappa_a \approx \kappa_b$ and $\Gamma_a \approx \Gamma_b$, one can consider a simpler version of the stochastic differential eqs. (19) and (20) for which the dynamics of amplitudes A and B is

This is a pre-print version. Published in *Proceedings of the Royal Society A* (2013) Volume 469, Issue 2151, Article number 20120535, DOI: 10.1098/rspa.2012.0535

governed by a potential $V(A,B)$:

$$\begin{aligned}\dot{A} &\simeq -\frac{\partial V}{\partial A} + \zeta_a,\\ \dot{B} &\simeq -\frac{\partial V}{\partial B} + \zeta_b,\end{aligned} \tag{25}$$

with

$$V(A,B) = -\frac{\nu_a}{2}A^2 - \frac{\nu_b}{2}B^2 + \frac{9\kappa}{128}\left(A^4+B^4\right) + \frac{3\kappa}{64}A^2B^2 - \frac{\Gamma}{4\omega_n^2}\ln(AB). \tag{26}$$

For such system, the stationary probability density function solution of the associated Fokker-Planck equation is given by

$$P(A,B) \quad = \quad \frac{1}{\mathcal{N}}\exp\left(-\frac{4\omega_n^2}{\Gamma}V(A,B)\right), \tag{27}$$

where $\mathcal{N}$ is a normalization constant. Making use of the values obtained for ν_a, ν_b, κ and Γ from the system identification process presented in the previous section, the potentials and corresponding density functions were computed according to eqs. (26) and (27). The results are presented in fig. 6. One can observe a fairly good agreement between the bivariate density functions from subfigures 3(a) and 3(c) and the ones in subfigures 6(a) and 6(c) given by the simplified theoretical model which does not take into account the phase dynamics and which is fed with the best fit parameters from the previous section. This is again a clear indication that the stochastic differential system (18) allows to properly model the dynamics of azimuthal eigenmodes in real gas turbine annular combustors.

One can also note that for $\nu_a = \nu_b$, the *deterministic* part of the model has been already analyzed by [17] from a theoretical point of view. Indeed when $\nu_a = \nu_b$ and $\Gamma_a = \Gamma_b = 0$ the simplified version (25) of the coupled system (18) belongs to region II in figures 14 and 15 of the aforementioned study. [17] focused on the bifurcations encountered with dynamical system exhibiting $O(2)$ symmetry which are particularly relevant in fluid dynamics where the symmetry often plays a crucial role, yielding standing or travelling waves (e.g. [26]). Another example of study dealing with this set of coupled amplitude equations is the one from [3], tackling with the nonlinear interaction of non-resonant modes in pulsating stars (see also [4]). [5] also investigated the influence of stochastic forcing on the modal dynamics of these stars.

In the present work, it is shown that the stochastic forcing produced by the turbulent combustion noise induces intermittent transitions between standing and spinning acoustic modes. As noticed by one of the reviewers of this work, this phenomenon resembles to the reversals of the geomagnetic poles which may be explained in terms of symmetry-breaking bifurcations submitted to turbulent fluctuations as shown by [27]. One can also refer to [22], [30] and [2].

6. Discussion

The thermoacoustic coupling in annular combustion chambers commonly encountered in gas turbine applications has been investigated throughout this paper. The aim was to address a question

This is a pre-print version. Published in *Proceedings of the Royal Society A* (2013) Volume 469, Issue 2151, Article number 20120535, DOI: 10.1098/rspa.2012.0535

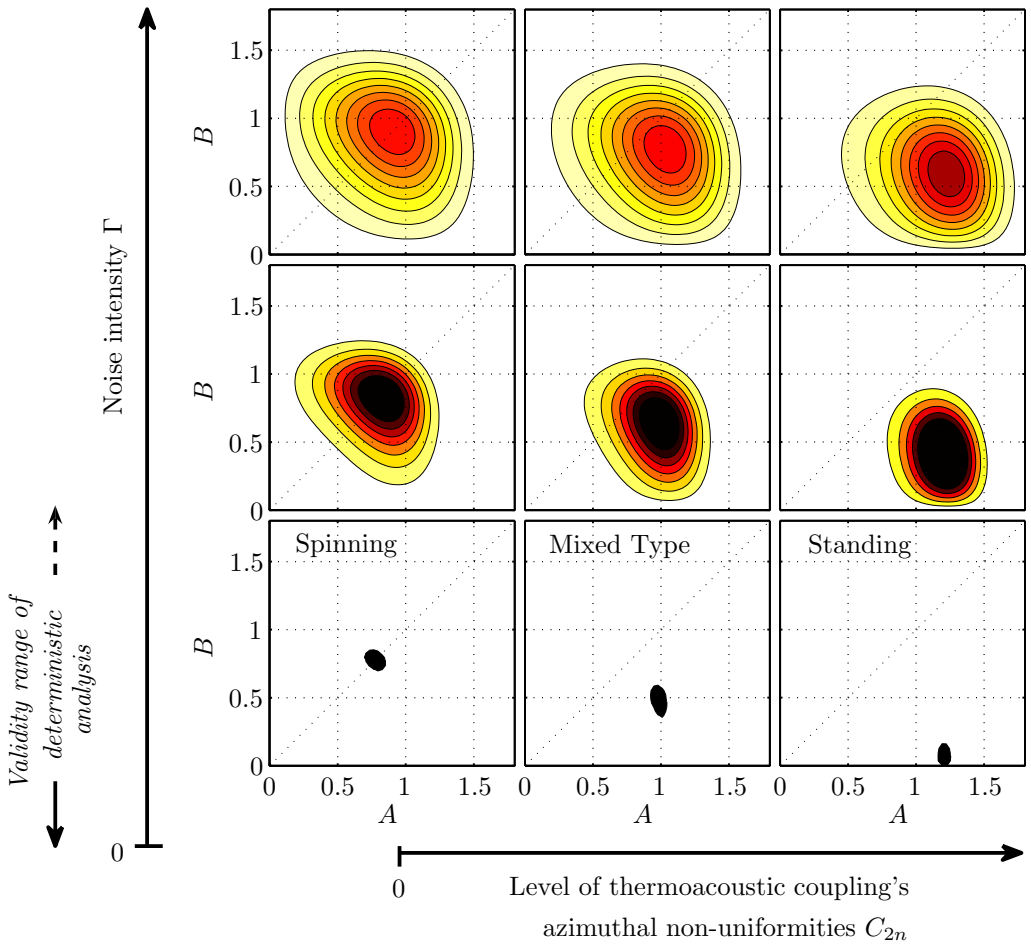

Figure 7: Examples of bivariate density functions of the modal amplitudes A and B calculated from eq. (27) for different noise intensities Γ and azimuthal non-uniformity levels C_{2n} and for fixed linear growth rate ν and nonlinearity coefficient κ (see [24] for the definition of C_{2n}; $\nu_a = \nu(1 + C_{2n})$ and $\nu_b = \nu(1 - C_{2n})$) . **Bottom row:** $\Gamma \to 0$, deterministic approach can be used. When $C_{2n} = 0$, i.e. uniform azimuthal distribution of the nonlinear thermo-acoustic coupling, a purely spinning mode establish in the annular chamber. When $C_{2n} \neq 0$, i.e. non-uniform azimuthal distribution, the mode exhibits either a combined spinning/standing dynamics or a purely standing oscillation. **Middle and top rows:** the noise level cannot be neglected, deterministic prediction are not anymore valid and stochastic analysis is needed.

This is a pre-print version. Published in *Proceedings of the Royal Society A* (2013) Volume 469, Issue 2151, Article number 20120535, DOI: 10.1098/rspa.2012.0535

raised in several recent publications: Do the azimuthal modes rotate or stand in the annular combustor of a gas turbine? Three points clarifying that question can be retained from this study:

1. From the time-resolved acoustic field reconstructed from measurements on a heavy-duty gas turbine combustor, it has been observed that limit cycles intermittently switch between spinning and standing modes. Bivariate probability density plots reveal wide distributions of modal amplitudes and phases with clearly defined maxima.
2. The standing and spinning modes have been previously predicted using a deterministic analysis. However the deterministic approach cannot predict the switching behavior between spinning and standing oscillations. This is because in industrial applications, the background noise produced by the highly turbulent reactive flow is very intense, stochastically perturbs the limit cycles and cannot be neglected when one intend to describe modal dynamics.
3. The system of three coupled stochastic differential equations describing modal amplitudes and phases is able to capture the properties of the dynamic pressure field which results from combined nonlinear thermoacoustic coupling and random perturbations by the non-coherent combustion noise.

One can also add that in order to meet component lifetime requirements in real gas turbine applications, the combustion is adjusted in such a manner that high amplitude pulsations are avoided. As a consequence a practical gas turbine does not operate far away from the Hopf bifurcation point. Hence the stochastic forcing of the limit cycles cannot be neglected. In turn, the modal dynamics results from the balance between the robustness of the limit cycle established in the chamber and the non-negligible stochastic forcing strength. Standing oscillations sporadically alternate with spinning ones with preferred locking positions defined by the azimuthal non-uniformities of the thermoacoustic strength. One can refer to figure 7 to get an overview of the various situations which can be encountered when considering thermoacoustic coupling in annular combustion chambers. Note that these probability density functions were calculated from the simplified version (25) of the coupled system (18) which does not include phase dynamics.

References

[1] Balanov, A., Janson, N., Postnov, D., and Sosnovtseva, O. (2009). *Synchronization – From Simple to Complex*. Springer-Verlag Berlin Heidelberg.

[2] Bordja, L., Tuckerman, L. S., Witkowski, L. M., Navarro, M. C., Barkley, D., and Bessaih, R. (2010). Influence of counter-rotating von kármán flow on cylindrical rayleigh-bénard convection. *Physical Review E*, **81**, 036322.

[3] Buchler, J. R. (1993). A dynamical systems approach to nonlinear stellar pulsations. In *Nonlinear Phenomena in Stellar Variability*, ed. M. Takeuti & J. R. Buchler (Dordrecht: Kluwer; reprinted from 1993, Ap& SS, 210, 1).

[4] Buchler, J. R. and Kolláth, Z. (2011). On the blazhko effect in rr lyrae stars. *The astrophysical journal*, **731:24**, 4pp.

[5] Buchler, J. R., Goupil, M.-J., and Kovacs, G. (1993). Stellar pulsations with stochastic driving. *Atron. Astrophys.*, **280**, 157–168.

This is a pre-print version. Published in *Proceedings of the Royal Society A* (2013) Volume 469, Issue 2151, Article number 20120535, DOI: 10.1098/rspa.2012.0535

[6] Clavin, P., Kim, J. S., and Williams, F. A. (1994). Turbulence-induced noise effects on high-frequency combustion instabilities. *Combust. Sci. Tech.*, **96**, 61–84.

[7] Eroglu, A., Flohr, P., Brunner, P., and Hellat, J. (2009). Combustor design for low emissions and long lifetime requirements. In *Proceedings of the ASME Turbo Expo*, volume 2, pages 435–444.

[8] Evesque, S., Polifke, W., and Pankiewitz, C. (2003). Spinning and azimuthally standing acoustic modes in annular combustors. In *Proceedings of the 9^{th} AIAA/CEAS Aeroacoustics Conference, Paper AIAA 2003-3182*, Hilton Head, South Carolina.

[9] Honisch, C. and Friedrich, R. (2011). Estimation of kramers-moyal coefficients at low sampling rates. *Physical Review E - Statistical, Nonlinear, and Soft Matter Physics*, **83**(6).

[10] Hurle, I. R., Price, R. B., Sudgen, T. M., and Thomas, A. (1968). Sound emission from open turbulent premixed flames. *Proc. Roy. Soc. A*, **303**, 409–427.

[11] Kolmogorov, A. N. (1931). Über die analytischen methoden in der wahrscheinlichkeitsrechnung. *Math. Ann.*, **140**, 415–458.

[12] Krebs, W., Flohr, P., Prade, B., and Hoffmann, S. (2002). Thermoacoustic stability chart for high intensity gas turbine combustion system. *Combust. Sci. Technol.*, **174**(7), 99–128.

[13] Krylov, N. and Bogoliubov, N. (1949). *Introduction to nonlinear mechanics*. Princeton University Press.

[14] Lade, S. J. (2009). Finite sampling interval effects in kramers-moyal analysis. *Physics Letters, Section A: General, Atomic and Solid State Physics*, **373**(41), 3705–3709.

[15] Lieuwen, T. C. (2003). Statistical characteristics of pressure oscillations in a premixed combustor. *J. Sound Vib.*, **260**, 3–17.

[16] Lighthill, M. J. (1952). On sound generated aerodynamically. i. general theory. *Proc. R. Soc. Lond. Ser. A – Math. Phys. Sci.*, **211**, 565–587.

[17] Marques, F., Lopez, J. M., and Blackburn, H. M. (2004). Bifurcations in systems with z_2 spatio-temporal and o(2) spatial symmetry. *Physica D*, **189**, 247–276.

[18] Moeck, J. P. (2010). *Analysis, Modeling, and Control of Thermoacoustic Instabilities*. Doctoral thesis, Technische Universität Berlin, http://opus.kobv.de/tuberlin/volltexte/2010/2815/pdf/moeck_jonas.pdf.

[19] Moeck, J. P. and Paschereit, C. O. (2009). Modeling thermoacoustic instabilities in an annular rijke tube: Asymmetries and standing and spinning modes. In *ICSV 16^{th} Proceedings*, Krakòw, Poland.

[20] Moeck, J. P., Paul, M., and Paschereit, C. O. (2010). Thermoacoustic instabilities in an annular rijke tube. In *Proceedings of the ASME Turbo Expo*, volume 2, pages 1219–1232.

[21] Morgans, A. S. and Stow, S. R. (2007). Model-based control of combustion instabilities in annular combustors. *Combust. & Flame*, **150**, 380–399.

[22] Mujica, N. and Lathrop, D. P. (2006). Hysteretic gravity-wave bifurcation in a highly turbulent swirling flow. *J. Fluid Mech.*, **551**, 49–63.

[23] Noiray, N. and Schuermans, B. (2012). Deterministic quantities characterizing noise driven hopf bifurcations in gas turbine combustor. *Int. J. Non-linear Mechanics*, **in press**, http://dx.doi.org/10.1016/j.ijnonlinmec.2012.11.008.

[24] Noiray, N., Bothien, M., and Schuermans, B. (2011). Investigation of azimuthal staging concepts in annular gas turbine. *Comb. Theory and Modelling*, **15**(5), 585–606.

[25] Oberleithner, K., Schimek, S., and Paschereit, C. O. (2012). On the impact of shear layer instabilities on global heat release rate fluctuations: linear stability analysis of an isothermal and a reacting swirling jet. In *Proceedings of the ASME Turbo Expo, GT2012-69774*.

[26] Panades, C., Marques, F., and Lopez, J. M. (2011). Transitions to three-dimensional flows in

This is a pre-print version. Published in *Proceedings of the Royal Society A* (2013) Volume 469, Issue 2151, Article number 20120535, DOI: 10.1098/rspa.2012.0535

a cylinder driven by oscillations of the sidewall. *J. Fluid Mech.*, **681**, 515–536.

[27] Pétrélis, F., Fauve, S., Dormy, E., and Valet, J. P. (2009). Simple mechanism for reversals of earth's magnetic field. *Phys. Rev. Letters*, **102**, 144503.

[28] Poinsot, T., Wolf, P., Staffelbach, G., Gicquel, L. Y. M., and Muller, J. D. (2011). Identification of azimuthal modes in annular combustion chambers. *Center for Turbulence Research Annual Research Briefs 2011*, pages 249–258.

[29] Rajaram, R. and Lieuwen, T. (2009). Acoustic radiation from turbulent premixed flames. *Journal of Fluid Mechanics*, **637**, 357–385.

[30] Ravelet, F., Berhanu, M., Monchaux, R., Aumaître, S., Chiffaudel, A., Daviaud, F., Dubrulle, B., Bourgoin, M., Odier, P., Plihon, N., Pinton, J.-F., Volk, R., Fauve, S., Mordant, N., and Pétrélis, F. (2008). Chaotic dynamos generated by a turbulent flow of liquid sodium. *Phys. Rev. Letters*, **101**, 074502.

[31] Rayleigh, L. (1896). *The Theory of Sound*. MacMillan, 2nd edition, Vol. 2, pp 224–234, London.

[32] Roberts, J. B. and Spanos, P. D. (1986). Invited review no. 1: Stochastic averaging: an approximate method of solving random vibration problems. *Int. J. Non-linear Mechanics*, **21**(2), 111–134.

[33] Schuermans, B., Paschereit, C. O., and Monkewitz, P. (2006). Non-linear combustion instabilities in annular gas turbine combustors. In *AIAA paper 2006-0549, 44^{th} AIAA Aerospace sciences meeting and exhibit*, Reno, Nevada.

[34] Seume, J. R., Vortmeyer, N., Krause, W., Hermann, J., Hantschk, C., Zangl, P., Gleis, S., Vortmeyer, D., and Orthmann, A. (1998). Application of active combustion instability control to a heavy duty gas turbine. *Journal of Engineering for Gas Turbines and Power*, **120**(4), 721–726.

[35] Siegert, S., Friedrich, R., and Peinke, J. (1998). Analysis of data sets of stochastic systems. *Physics Letters A*, **243**, 275–280.

[36] Spanos, P.-T. D. (1978). Stochastic analysis of oscillators with non-linear damping. *Int. J. Non-linear Mechanics*, **13**, 249–259.

[37] Staffelbach, G., Gicquel, L. Y. M., Boudier, G., and Poinsot, T. (2009). Large eddy simulation of self excited azimuthal modes in annular combustors. *Proc. Combust. Inst.*, **32**, 2909–2916.

[38] Stow, S. R. and Dowling, A. P. (2009). A time-domain network model for nonlinear thermoacoustic oscillations. *Journal of Engineering for Gas Turbines and Power*, **131**(3).

[39] Stratonovich, R. C. (1963). *Topics in the theory of random noise, Vol. 2*. Gordon & Breach, New-York.

[40] Waugh, I. C., Geuss, M., and Juniper, M. P. (2011). Triggering, bypass transition and the effect of noise on a linearly stable thermoacoustic system. *Proc. Combust. Inst.*, **33**, 2945–2952.

[41] Wolf, P., Staffelbach, G., Roux, A., Gicquel, L., Poinsot, T., and Moureau, V. (2009). Massively parallel les of azimuthal thermo-acoustic instabilities in annular gas turbines. *Comptes Rendus - Mecanique*, **337**(6-7), 385–394.

[42] Wolf, P., Staffelbach, G., Gicquel, L., Müller, J., and Poinsot, T. (2012). Acoustic and large eddy simulation studies of azimuthal modes in annular combustion chambers. *Combustion and Flame*, **159**, 3398–3413.

This is a pre-print version. Published in *Proceedings of the Royal Society A* (2013) Volume 469, Issue 2151, Article number 20120535, DOI: 10.1098/rspa.2012.0535